

Single-qubit lasing in the strong-coupling regime

Stephan André,^{1,2} Pei-Qing Jin,¹ Valentina Brosco,^{1,3} Jared H. Cole,¹
Alessandro Romito,^{1,4} Alexander Shnirman,^{5,2} and Gerd Schön^{1,2}

¹*Institut für Theoretische Festkörperphysik, Karlsruhe Institute of Technology, 76128 Karlsruhe, Germany*

²*DFG Center for Functional Nanostructures (CFN),*

Karlsruhe Institute of Technology, 76128 Karlsruhe, Germany

³*Dipartimento di Fisica, Università “La Sapienza”, P.le A. Moro 2, 00185 Roma, Italy*

⁴*Freie Universität Berlin, Fachbereich Physik, Arnimallee 14, 14195 Berlin, Germany*

⁵*Institut für Theorie der Kondensierten Materie,*

Karlsruhe Institute of Technology, 76128 Karlsruhe, Germany

(Dated: October 16, 2018)

Motivated by recent “circuit QED” experiments we study the lasing transition and spectral properties of single-qubit lasers. In the strong coupling, low-temperature regime quantum fluctuations dominate over thermal noise and strongly influence the linewidth of the laser. When the qubit and the resonator are detuned, amplitude and phase fluctuations of the radiation field are coupled, and the phase diffusion model, commonly used to describe conventional lasers, fails. We predict pronounced effects near the lasing transition, with an enhanced linewidth and non-exponential decay of the correlation functions. We cover a wide range of parameters by using two complementary approaches, one based on the Liouville equation in a Fock state basis, covering arbitrarily strong coupling but limited to low photon numbers, the other based on the coherent-state representation, covering large photon numbers but restricted to weak or intermediate coupling.

PACS numbers:

I. INTRODUCTION

A strong, coherent coupling between a superconducting qubit and an electrical resonator was first realized experimentally by Wallraff *et al.* and Chiorescu *et al.* [1, 2]. Their work stimulated substantial theoretical [3–9] and experimental activities [10–16] devoted to the study of further quantum electrodynamic effects in electric circuits. In these “circuit QED” setups a superconducting qubit plays the role of an artificial atom, while the radiation field is replaced by the modes of an electric resonator. In some of these experiments a strong enhancement of the resonator field and lasing were observed [14, 15].

In contrast to conventional lasers where many atoms are coupled weakly to the light field in an optical interferometer, in the single-qubit laser a single superconducting qubit is coupled strongly to the microwave field of the resonator circuit. Furthermore, typical circuit QED setups operate at low temperatures, where thermal noise is weak and quantum fluctuations, arising from the qubit-resonator coupling, become dominant [17–19].

In this work we study the lasing transition and the spectral properties of single-qubit lasers focusing on the regime of strong qubit-resonator coupling at low temperatures. In this regime we find qualitatively new behavior of the laser linewidth. In earlier work [20, 21] we observed that the linewidth depends in a non-monotonous way on the coupling strength: approaching the lasing transition from weak coupling one observes the well-known linewidth narrowing. However, for stronger coupling the linewidth of the single-qubit laser increases again, and the lasing state deteriorates, a behavior not observed in conventional lasers.

If the qubit and the laser are detuned from resonance we find an even more surprising behavior: The linewidth, which generally increases with detuning, is strongly enhanced near the lasing transition, and for strong coupling or low damping rate of the resonator shows a local maximum as a function of detuning. In this regime, the correlation functions of the resonator decay non-exponentially in time. As we demonstrate below, this behavior is due to the coupling between phase and amplitude fluctuations, which are neglected in the commonly used phase diffusion model [22].

In order to cover a wide range of parameters we analyze the properties of the laser using two approaches. One is based on a numerical analysis of the Liouville equation in a basis of Fock states. It allows for arbitrarily strong coupling but is limited by the size of the basis which we can handle. This puts constraints on the thermal photon number and the quality factor of the resonator. The other is based on the coherent-state representation. It covers large photon numbers (and thus low damping rate of the resonator) but fails in the strong coupling regime. The results of the two approaches coincide well in an interesting overlapping parameter regime.

The paper is organized as follows: In Sec. II, we describe the model and in Sec. III the two approaches employed to solve the master equation. Stationary properties, such as the average photon number are evaluated in Sec. IV. In the central part of this paper, Sec. V, we investigate the spectral function and the linewidth near the lasing transition in the frame of the two approaches. The consequences of amplitude fluctuations and the failure of the phase diffusion model are discussed. We draw conclusions in Sec. VI.

II. THE MODEL

The single-qubit laser realized by Astafiev et al. [14] consists of a Cooper pair box (CPB) [23], characterized by the charging energy scale E_{ch} and the Josephson coupling energy E_J , which is coupled capacitively to a superconducting coplanar waveguide resonator with frequency ω_R . In the regime typically explored in the experiments, only two charge states of the CPB, indicated as $|0\rangle$ and $|2\rangle$ and differing by one Cooper pair, are coherently and (near) resonantly coupled to the cavity. In this situation, the system can be modelled as a two-level system (qubit) coupled to a harmonic oscillator with Hamiltonian [3]

$$H = -\frac{1}{2}(E_{\text{ch}}\hat{\tau}_z + E_J\hat{\tau}_x) + \hbar\omega_R a^\dagger a + \hbar g_0 \hat{\tau}_z (a + a^\dagger). \quad (1)$$

Here we set $\hat{\tau}_z = |0\rangle\langle 0| - |2\rangle\langle 2|$, $\hat{\tau}_x = |0\rangle\langle 2| + |2\rangle\langle 0|$, while a and a^\dagger are the annihilation and creation operators of photons in the resonator. The qubit-resonator coupling strength is denoted by g_0 . In the considered single-qubit laser experiments, the qubit level spacing and ω_R are in the range of 10 GHz (i.e., microwave frequencies) while the strength of the coupling g_0 reaches 100 MHz. This is much stronger than usual for conventional lasers but still small enough to allow for the rotating-wave approximation. Switching to the qubit's eigenbasis we can recast the Hamiltonian in the Jaynes-Cummings form [24],

$$H_{\text{JC}} = \frac{1}{2}\hbar\omega_Q\sigma_z + \hbar\omega_R a^\dagger a + \hbar g (\sigma_+ a + \sigma_- a^\dagger). \quad (2)$$

Here we introduce new Pauli matrices, $\sigma_{x,y,z}$ and $\sigma_\pm = \sigma_x \pm i\sigma_y$. Furthermore, the the qubit's level spacing $\hbar\omega_Q = \sqrt{E_{\text{ch}}^2 + E_J^2}$ and the effective coupling strength $g = \sin\theta g_0$ with $\theta = -\arctan(E_J/E_{\text{ch}})$ have been introduced. In the following we allow the qubit and the resonator to be detuned by $\Delta = \omega_Q - \omega_R$. Although we consider the experiment of Ref. [14] as a motivation for this analysis, our model also applies to many further circuit QED experiments in the lasing regime [5].

As discussed in detail in Refs. [21, 25], the pumping mechanism implemented by Astafiev et al. [14] depends on current injection in a superconducting single-charge transistor and actually involves three charge states. Besides the states $|0\rangle$ and $|2\rangle$, also a one-excess-electron charge state is incoherently coupled to the system and excited via an external voltage bias. For the present discussion it is sufficient to model this driving simply by adding an incoherent excitation term to the qubit's dynamics.

In this case, within the usual Markov approximation, for weak system-environment coupling and using the secular approximations, we can analyze the dynamics of a single-qubit laser in the frame of a Bloch-Redfield master equation [26, 27]. The reduced qubit-resonator density matrix ρ obeys the master equation in Lindblad form [28], which in the laboratory frame reads

$$\dot{\rho} = -\frac{i}{\hbar}[H_{\text{JC}}, \rho] + \mathcal{L}_Q \rho + \mathcal{L}_R \rho. \quad (3)$$

Here the Liouville super-operators \mathcal{L}_R and \mathcal{L}_Q account for the resonator's and the qubit's dissipative processes,

$$\begin{aligned} \mathcal{L}_R \rho = & \frac{\kappa}{2}(N_{\text{th}} + 1) (2a\rho a^\dagger - a^\dagger a\rho - \rho a^\dagger a) \\ & + \frac{\kappa}{2}N_{\text{th}} (2a^\dagger \rho a - a a^\dagger \rho - \rho a a^\dagger), \end{aligned} \quad (4)$$

and

$$\begin{aligned} \mathcal{L}_Q \rho = & \frac{\Gamma_\varphi^*}{2} (\sigma_z \rho \sigma_z - \rho) \\ & + \frac{\Gamma_\downarrow}{2} (2\sigma_- \rho \sigma_+ - \rho \sigma_+ \sigma_- - \sigma_+ \sigma_- \rho) \\ & + \frac{\Gamma_\uparrow}{2} (2\sigma_+ \rho \sigma_- - \rho \sigma_- \sigma_+ - \sigma_- \sigma_+ \rho). \end{aligned} \quad (5)$$

The dissipative dynamics of the resonator depends on the bare damping rate κ and the thermal photon number N_{th} , while the qubit's dynamics is described by excitation, relaxation, and pure dephasing with rates Γ_\uparrow , Γ_\downarrow , and Γ_φ^* , respectively. For later use, we also introduce the inverse of the T_1 time, $\Gamma_1 = \Gamma_\uparrow + \Gamma_\downarrow$, the total dephasing rate $\Gamma_\varphi = \Gamma_1/2 + \Gamma_\varphi^*$, as well as the bare population inversion of the qubit $\tau_0 = (\Gamma_\uparrow - \Gamma_\downarrow)/\Gamma_1$.

As mentioned in the Introduction, in single-qubit lasers the lasing transition and state depend on the coupling strength g and the qubit-resonator detuning Δ . In order to characterize the lasing state in these systems we, therefore, study the stationary properties of the radiation field, such as average photon number and photon number fluctuations as a function of these parameters. To fully characterize the lasing state we further investigate the emission spectrum of the field,

$$S_e(\omega) = \int_{-\infty}^{\infty} dt e^{-i\omega t} \langle a^\dagger(t)a(0) \rangle, \quad (6)$$

and the linewidth of the laser radiation. This allows us to describe the transition between the incoherent and the coherent state of the resonant cavity and to draw a phase diagram of the lasing state.

III. METHODS

We address the lasing state and the resonator spectrum by two different methods, by a direct numerical diagonalization of the master equation for the density matrix and by a Fokker-Planck equation approach. The two methods cover different parameter regimes and provide complementary physical pictures.

A. Direct integration of the Liouville equation (DILE)

After projecting on the Fock states basis, we can recast the master equation (3) in vector form

$$\dot{\vec{\rho}} = G\vec{\rho}. \quad (7)$$

The reduced density matrix ρ is arranged as a vector $\vec{\rho}$, and G is a superoperator acting in the space of the system operators. This form is convenient for the numerical evaluation of both static and spectral properties of the field.

From the stationary solution of the master equation $G\vec{\rho}_s = 0$ we obtain equilibrium values such as, e.g., the photon number in the resonator, $\langle n \rangle = \text{Tr}\{a^\dagger a \rho_s\}$. From Eq. (7) we can also derive expressions for time-dependent correlation functions [29], e.g., $\langle a^\dagger(t)a(0) \rangle$. In order to do so, we employ the quantum regression theorem [28, 30]

$$\langle a^\dagger(t)a(0) \rangle = \text{Tr}\{a^\dagger e^{Gt} a \rho_s\}. \quad (8)$$

To proceed it is convenient to diagonalize the superoperator G and express the product $a \rho_s$ in terms of eigenvectors of G , $a \rho_s = \sum_k c_k \vec{v}_k$. Acting on the equation with the exponential $\exp(Gt)$ leads to

$$e^{Gt} a \rho_s = \sum_k c_k e^{\lambda_k t} \vec{v}_k,$$

where λ_k is the eigenvalue corresponding to the eigenvector \vec{v}_k . Once the eigenvalues λ_k and expansion coefficients c_k are known, we can easily obtain the correlation function for all times t .

We solved Eqs. (7) and (8) numerically with results to be presented below. For this purpose we truncate the Hilbert space of the resonator to a finite number N of photon number states. In this case the superoperator G is represented by a $4N^2 \times 4N^2$ -matrix, growing fast with N , which limits the method in our case to $N \leq 30$. This puts constraints to the values of rates κ and Γ_1 . As will be shown in Sec. IV, the average photon number $\langle n \rangle$ in the resonator obeys the relation $\langle n \rangle \lesssim \Gamma_1/(2\kappa)$. Hence the damping rate κ should not be too small, i.e., $\kappa \gtrsim \Gamma_1/N$. On the other hand, for the calculation of average steady state values, as well as for the linewidth exactly at resonance ($\Delta = 0$), the calculations reduce to solving a system of linear equations. In these cases, we can cover a much higher number of photon number states, $N \lesssim 200$.

B. Fokker-Planck equation (FPE)

Alternatively, following the route outlined in Ref. [28], we can derive a Fokker-Planck equation for the single qubit-laser in the coherent state representation. In this case we represent the qubit-oscillator density matrix as $\rho(t) = \int d^2\alpha \tilde{\rho}(\alpha, t) |\alpha\rangle\langle\alpha|$, where $\tilde{\rho}(\alpha, t)$ is a 2×2 matrix in the qubit basis states. Substituting this expansion into Eq. (3) we obtain a master equation for the operator $\tilde{\rho}(\alpha, t)$. Its trace, $\text{Tr}_Q [\tilde{\rho}(\alpha, t)] \equiv P(\alpha, t)$, yields the probability for the radiation field to be in a coherent state $|\alpha\rangle$.

In typical experimental configurations [14], the dynamics of the qubit are much faster than that of the resonator. As a result the qubit decays on short time scales

to a quasi-steady state, which still depends on the slowly varying state of the radiation field $\alpha(t)$. We can adiabatically eliminate the qubit's degrees of freedom via a projective technique [28]. The resulting FPE contains a noise term arising from the qubit fluctuations. Generally, this noise term contains all orders of derivatives $\partial/\partial\alpha$ and $\partial/\partial\alpha^*$. If the coupling is weak compared to the dephasing rate of the qubit, $g \ll \Gamma_\varphi$, the noise term can be truncated to second order derivatives, and the resulting FPE in the rotating frame reads [28]

$$\frac{\partial P}{\partial t} = \frac{\kappa}{2} \left\{ \frac{\partial}{\partial\alpha} \left[\alpha - \frac{\alpha(1 - i\Delta/\Gamma_\varphi)C_0}{(1 + \Delta^2/\Gamma_\varphi^2)(1 + |\alpha|^2/n_0)} \right] + \frac{\partial^2}{\partial\alpha\partial\alpha^*} (N_{\text{th}} + Q) + \frac{\partial^2}{\partial\alpha^2} R + \text{c.c.} \right\} P. \quad (9)$$

Here $C_0 = 2g^2\tau_0/(\kappa\Gamma_\varphi)$ and $n_0 = \Gamma_1\Gamma_\varphi/(4g^2)$. The resonator-qubit coupling leads to the noise terms

$$Q = \frac{g^2}{\kappa} \text{Re} \left[\int_0^\infty dt (\langle \sigma_+(t)\sigma_-(0) \rangle_{\text{q}} - \langle \sigma_+ \rangle_{\text{q}} \langle \sigma_- \rangle_{\text{q}}) \right],$$

$$R = -\frac{g^2}{\kappa} \int_0^\infty dt (\langle \sigma_-(t)\sigma_-(0) \rangle_{\text{q}} - \langle \sigma_- \rangle_{\text{q}}^2), \quad (10)$$

which can be again calculated using the quantum regression theorem [28, 30]. Here $\langle \dots \rangle_{\text{q}}$ denotes the average over the qubit in the quasi-steady state.

To proceed we introduce polar coordinates r and φ , denoting the amplitude and phase of the radiation field in a coherent state, respectively. In the stationary limit, we expect that the field distribution function is independent of the phase. Hence we seek for the solutions $\lim_{t \rightarrow \infty} P(\alpha, t) = P_s(r)$. In this way we obtain for the steady-state distribution

$$P_s(r) = N e^{-\Phi(r)}, \quad (11)$$

normalized such that $2\pi \int dr r P_s(r) = 1$. The expression for $\Phi(r)$ along with further details of the derivation is given in appendix A.

The correlation function of the resonator $\langle a^\dagger(t)a(0) \rangle$ can be calculated by introducing the conditional probability $P(r, \varphi, t/r_0, \varphi_0, 0)$ for the radiation field to be in the coherent state (r, φ) at time t , given that it was in the state (r_0, φ_0) at $t = 0$. In terms of distribution functions, the correlation function is given by [31]

$$\begin{aligned} \langle a^\dagger(t)a(0) \rangle &= \int dr r^2 \int d\varphi d\varphi_0 dr_0 r_0^2 P_s(r_0) \\ &\quad \times e^{i(\varphi_0 - \varphi)} P(r, \varphi, t/r_0, \varphi_0, 0) \\ &\equiv \int dr r^2 W(r, t), \end{aligned} \quad (12)$$

where $W(r, t)$ obeys the differential equation

$$\partial W / \partial t = \hat{L} W. \quad (13)$$

The explicit form of the differential operator \hat{L} can be obtained from the FPE equation [32] and it is given in appendix A. To solve Eq. (13) we discretize the amplitude

r and diagonalize the \hat{L} matrix on the resulting lattice. We can then expand $W(r, t) = \sum_k c_k \chi_k(r) e^{-\lambda_k t}$ in eigenfunctions of \hat{L} , where λ_k is the eigenvalue corresponding to the eigenfunction χ_k , and the coefficients c_k are determined by the initial condition $W(r, t = 0) = 2\pi r P_s(r)$.

Each of the two methods described so far, based on different representations of the density matrix, has its advantages and limitations. The Fock-state representation used in the direct integration of the Liouville equation is exact but, for practical reasons, can only deal with low photon numbers. The coherent-state representation and FPE approach provide insight into the distinction between the quantum and classical descriptions and can be employed in the large photon number limit. But the condition $g/\Gamma_\varphi \ll 1$ must be satisfied to allow truncating the derivatives to second order. Hence it fails when the coupling is too strong.

IV. PHASE DIAGRAM AND STATIONARY PROPERTIES

In this Section we investigate the stationary properties of single-qubit lasers for different values of the qubit-resonator coupling g and detuning Δ . In all results presented below we assume $N_{\text{th}} = 0$ and keep the bare qubit inversion fixed at $\tau_0 = 0.975$. The study presented here serves a two-fold purpose, on one hand it aims at characterizing the state of the radiation field in the different parameter regimes explored in the experiment [14], on the other hand it gives us the opportunity to compare the FPE and the DILE methods.

A. Lasing transition

In order to study the nature of the radiation field we first analyze the photon distribution function, $P_s(r)$, with results shown in Fig. 1. For weak coupling or large detuning the system is in the *thermal* regime, where the resonator behaves like a black-body cavity and $P_s(r)$ decays monotonically as a function of r (curve c in Fig. 1). Increasing the coupling strength or decreasing the detuning brings the system into a transition regime, where $P_s(r)$ has a maximum at a non-zero value of r , but the field still has some probability at $r = 0$ (curve b). A further change of parameters pushes the system into the lasing regime with a photon distribution having a negligible weight at $r = 0$. We note that the lasing threshold (solid line in Fig. 1) estimated within the semi-classical approximation [21],

$$\frac{2g^2\Gamma_\varphi}{\Gamma_\varphi^2 + \Delta^2} = \frac{\kappa}{\tau_0}, \quad (14)$$

coincides with the boundary of the thermal regime (found by evaluating whether the minimum of $\Phi(r)$ occurs at $r = 0$ [22]).

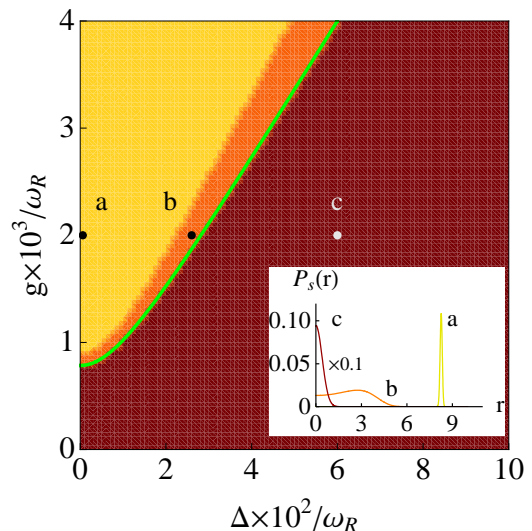


Figure 1: (Color online) Phase diagram (and in the inset distribution functions) in the lasing (light), non-lasing (dark) and the transition regimes (intermediate) as a function of the detuning $\Delta = \omega_Q - \omega_R$ and coupling g between qubit and resonator. The distribution functions are plotted with $\kappa = 10^{-4} \omega_R$, $g = 0.002 \omega_R$ and detuning $\Delta = 0$ at point a, $\Delta = 0.027 \omega_R$ at point b and $\Delta = 0.06 \omega_R$ at point c. Other parameters are $\Gamma_\varphi = 1.2 \times 10^{-2} \omega_R$, $\Gamma_1 = 1.6 \times 10^{-2} \omega_R$, $\tau_0 = 0.975$ and $N_{\text{th}} = 0$. The solid line represents the transition curve obtained from the semi-classical approximation.

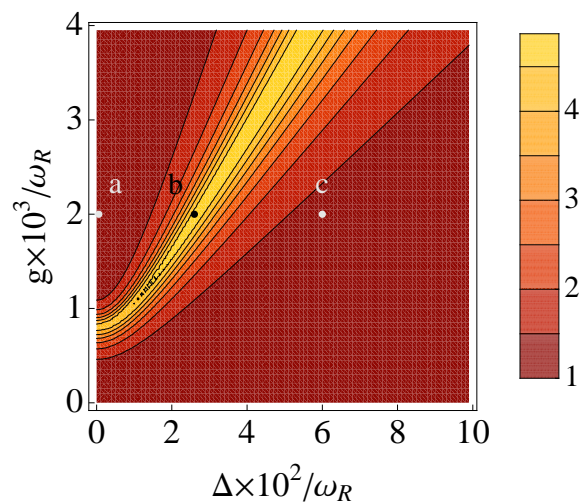


Figure 2: (Color online) Fano factor for different values of detuning and coupling between qubit and resonator. Points a, b, and c are defined as in Fig. 1.

A further hint at the nature of the radiation field in the different regimes is provided by the Fano factor $F = (\langle n^2 \rangle - \langle n \rangle^2) / \langle n \rangle$. As one may expect, deep in the thermal regime the photon distribution is simply a Bose distribution and, since $N_{\text{th}} = 0$, the Fano factor equals 1. As one approaches the transition regime, due to large

fluctuations in the photon number, the Fano factor is strongly enhanced, reaching a maximum in the transition region. Deep in the lasing regime, the field is in a coherent state and the Fano factor equals one again, $F \approx 1$. Fig. 2 shows that there is a wide region in the (Δ, g) -plane where F is significantly larger than 1. In this region, even well above the semi-classical lasing threshold, the field is not yet in a coherent state.

B. Photon number and fluctuations

The lasing transition is evident in the average photon number $\langle n \rangle$. Results are shown in Fig. 3 for varying coupling strength g . In the non-lasing regime, the photon number is small. Remarkably, even for a single-qubit laser $\langle n \rangle$ increases sharply near the threshold before it saturates deep in the lasing regime. Within the semi-classical approximation, the saturation photon number can be estimated as

$$\bar{n}_{\text{sat}} = \frac{\Gamma_1 \tau_0}{2\kappa}. \quad (15)$$

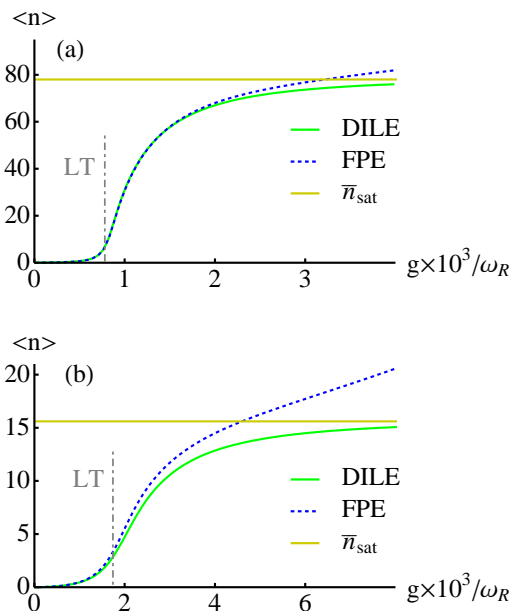


Figure 3: (Color online) Average photon number on resonance obtained from the DILE (solid) and the FPE approach (dotted). Parameters are $\kappa = 10^{-4} \omega_R$ in panel (a) and $\kappa = 5 \times 10^{-4} \omega_R$ in panel (b). The dot-dashed line indicates the lasing threshold (LT) estimated using Eq. (14).

In Fig. 3 we compare the results obtained from the DILE and FPE methods. Both coincide for weak coupling g . They differ when the coupling becomes stronger since the condition $g/\Gamma_\varphi \ll 1$ needed for the FPE approach is violated. The comparison of the two panels

in Fig. 3 shows that both approaches describe the lasing transition well if the bare damping rate of the resonator is weak (upper panel), but for a higher damping rate (lower panel) the FPE approach is not sufficient.

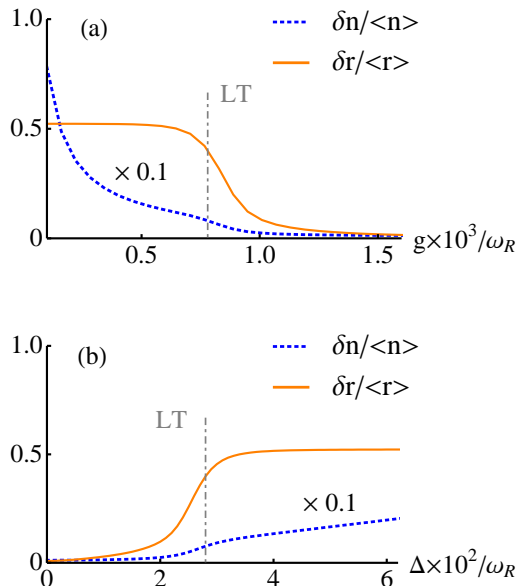


Figure 4: (Color online) Relative fluctuations as function of g at resonance (panel a) and as function of Δ at $g = 0.002 \omega_R$ (panel b). In both panels $\kappa = 10^{-4} \omega_R$.

Of interest for the following discussions are also the relative fluctuations of the photon number $\delta n / \langle n \rangle$ and of the field amplitude $\delta r / \langle r \rangle$ shown in Fig. 4. (For the parameters used, DILE and FPE coincide well.) The relative fluctuations, although they are rather weak in the lasing regime, have important effects on the spectral properties of the single-qubit laser, which we will discuss in the next section.

In the non-lasing regime, the correlations between the qubit and the resonator are negligible and the distribution function for the steady state can be approximated as $P_s(r) = \pi e^{-b r^2} / b$ with

$$b = \frac{\tau_0}{2(1 + \tau_0)} \left(1 - \frac{2\tau_0 \Gamma_\varphi}{\kappa} \frac{g^2}{\Gamma_\varphi^2 + \Delta^2} \right), \quad (16)$$

which is positive in this regime. The relative fluctuations of the photon number are thus given by $\delta n / \langle n \rangle = \sqrt{1 + b}$, which grow with decreasing g or increasing Δ . The relative amplitude fluctuations are constant in this regime, namely, $\delta r / \langle r \rangle = \sqrt{4/\pi - 1} \simeq 0.5$, as shown in Fig. 4.

V. LASER LINEWIDTH

This section is devoted to the study of the emission spectrum of the single-qubit laser radiation and the dependence of its linewidth on the qubit-resonator coupling

and detuning. Both in the FPE and the DILE approaches the correlation function of the resonator can be expanded as $\langle a^\dagger(t)a(0) \rangle = \sum_k \alpha_k \exp(-\lambda_k t)$, where $-\lambda_k$ are the eigenvalues of the discretized differential operator \hat{L} defined in Appendix A or of the superoperator G introduced in Section III A (both in the rotating frame), respectively. Using this expansion in Eq. (6) we obtain

$$S_e(\omega) = 2 \sum_k \frac{1}{[\omega + \text{Im}(\lambda_k)]^2 + [\text{Re}(\lambda_k)]^2} \times \{\text{Re}(\alpha_k)\text{Re}(\lambda_k) + \text{Im}(\alpha_k)[\omega + \text{Im}(\lambda_k)]\}. \quad (17)$$

This equation serves as starting point for the calculation of the resonator spectrum once the eigenvalues λ_k and the coefficients α_k are known.

Results for two different values of the detuning are plotted in Fig. 5. The spectrum is characterized by a linewidth, which we define - even in cases where the spectrum is not Lorentzian - to be the half-width at half-maximum (HWHM). We note that a detuning between qubit and resonator shifts the emission spectrum away from the bare frequency ω_R of the resonator. Near resonance, this frequency shift grows linearly with the detuning Δ [20, 21].

When analyzing the emission spectrum using the two approaches described above we arrive at the following main conclusions:

(i) The linewidth depends in a non-monotonous way on the coupling strength, consistent with Refs. 20, 21.

(ii) Away from resonance (but deep in the lasing regime), amplitude fluctuations contribute significantly to the linewidth. But they are neglected in the phase diffusion model.

(iii) For strong coupling or weak damping of the resonator the linewidth is strongly enhanced in the transition regime. In this case the emission spectrum is no longer purely Lorentzian.

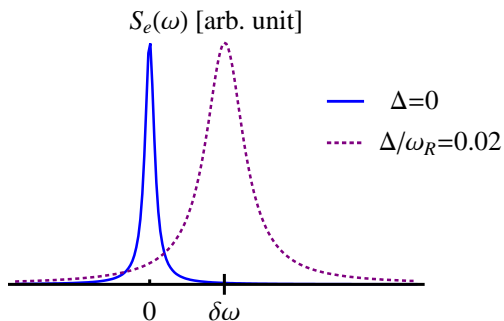


Figure 5: (Color online) Emission spectrum $S_e(\omega)$ in the rotating frame for $g = 0.003 \omega_R$ and $\kappa = 5 \times 10^{-4} \omega_R$. The frequency shift $\delta\omega$ at $\Delta = 0.02 \omega_R$ is about 0.56κ .

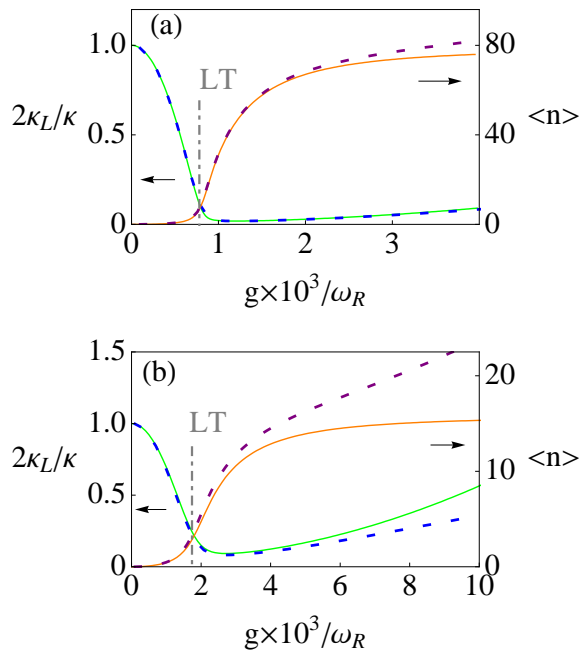


Figure 6: (Color online) Average photon number and linewidth as functions of the coupling strength on resonance with $\kappa = 10^{-4} \omega_R$ in panel (a) and $\kappa = 5 \times 10^{-4} \omega_R$ in panel (b). Results obtained from the DILE and the FPE methods are represented by the solid and the dashed lines, respectively.

A. Dependence on the coupling strength

One of the central results of Refs. 20, 21 was the non-monotonic dependence of the linewidth on the qubit-resonator coupling strength. This is demonstrated in Fig. 6, where the average photon number in the resonator and the linewidth of the emission spectrum are plotted as functions of the coupling strength g at resonance, $\Delta = 0$. We see that, while the photon number rapidly increases at the lasing transition and then saturates, the linewidth shows a non-monotonic behavior. For increasing but still weak coupling we observe the linewidth narrowing which is typical for lasers. However, in the deep lasing regime, the linewidth grows again with coupling strength, leading to a deterioration of the lasing state. This effect is very pronounced for low photon numbers in the resonator and strong coupling. In this regime, the linewidth can even become larger than the bare linewidth of the resonator.

As described in Sec. II, the DILE can be used if the photon number is not too high, i.e., if the damping rate κ of the resonator is not too small. On the other hand, the FPE approach requires that the coupling strength is much smaller than the dephasing rate of the qubit, $g \ll \Gamma_\varphi$. Figs. (3) and (6) show good agreement between both approaches for parameters where both are valid, i.e., for weak coupling and low photon number.

B. Linewidth as function of the detuning

At resonance (deep in the lasing regime), a satisfactory picture of the linewidth properties can be derived using the phase diffusion model (PDM) [22, 33]. Within this model the effects of amplitude fluctuations on the spectrum (see below) are neglected, and the linewidth coincides with the phase diffusion rate, which is only affected by phase fluctuations.

The PDM turns out to be no longer valid away from resonance when the quantum noise dominates. As shown in Fig. 7, when amplitude fluctuations are taken into account, the laser linewidth *increases* with growing detuning. This is obtained both in the DILE and the FPE approaches and in agreement with findings of Ref. 25. In contrast the PDM, although working well at resonance, predicts the wrong slope and curvature of the linewidth as a function of detuning.

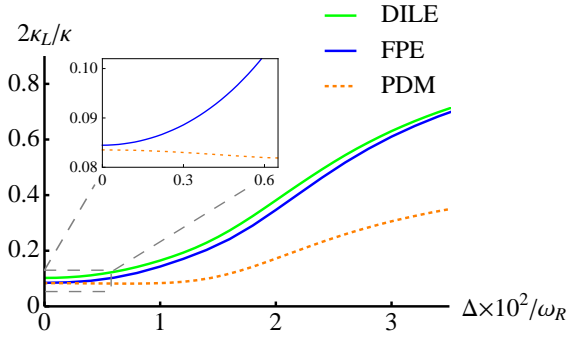


Figure 7: (Color online) Linewidth as a function of the detuning with $\kappa = 5 \times 10^{-4} \omega_R$, $g = 0.003 \omega_R$.

The failure of the PDM is due to the coupling of phase and amplitude fluctuations. In order to describe their effects on the linewidth, we consider the FPE in polar coordinates (see appendix A for details),

$$\begin{aligned} \frac{\partial P(r, \varphi, t)}{\partial t} &= \frac{\kappa}{4r} \frac{\partial}{\partial r} \left\{ [N_{\text{th}} + Q(r) + 2u(r)] r \frac{\partial}{\partial r} \right. \\ &\quad \left. + 4v(r) \frac{\partial}{\partial \varphi} + F(r) \right\} P(r, \varphi, t) \\ &\quad + \kappa \left(D_2(r) \frac{\partial^2}{\partial \varphi^2} + D_1(r) \frac{\partial}{\partial \varphi} \right) P(r, \varphi, t). \end{aligned} \quad (18)$$

The mixed derivative ($\propto \partial^2 / \partial r \partial \varphi$) couples the dynamics of phase and amplitude. The coefficient $v(r)$ is given by

$$v(r) = \text{Im} \left[e^{-2i\varphi} R(r, \varphi) \right]. \quad (19)$$

In the limit of full population inversion, $\tau_0 = 1$, and vanishing pure dephasing, $\Gamma_\varphi^* = 0$, it reduces to

$$v(r) = \frac{\Delta r^2 [(5 + \Delta^2 / \Gamma_\varphi^2) n_0 + 2r^2]}{4\kappa [(1 + \Delta^2 / \Gamma_\varphi^2) n_0 + r^2]^3}. \quad (20)$$

This form illustrates that the coupling term vanishes on resonance. But off-resonance in the lasing regime, $v(r)$ couples amplitude fluctuations to the phase dynamics and - as shown below - qualitatively influences the linewidth.

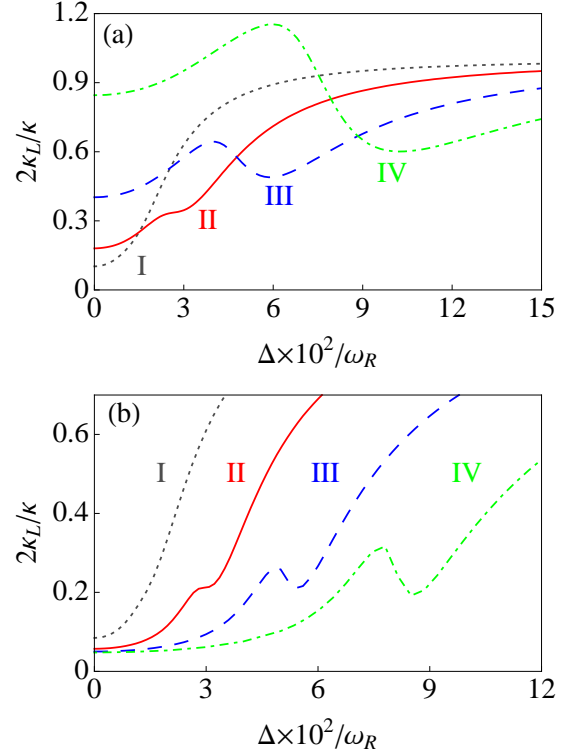


Figure 8: (Color online) Linewidth as functions of the detuning obtained from the DILE approach in panel (a) and from the FPE method in panel (b). Parameters are given in Table. I.

In the transition regime, the linewidth is enhanced and, as shown in Fig. 8, exhibits a peak structure for strong coupling or low damping of the resonator. This phenomenon arises due to the coupling of amplitude and phase fluctuations. For an estimate we expand $v(r)$ of Eq. (20) (neglecting pure dephasing and setting $\tau_0 = 1$) near the lasing transition in the small amplitude of the radiation field, $r^2 \ll \bar{n}_{\text{sat}}$. The result is $v(r) \simeq a_1 r^2 / \bar{n}_{\text{sat}}$ with expansion coefficient

$$a_1 = \frac{\sqrt{4\xi - 1}}{4\xi} (1 + \xi). \quad (21)$$

In the derivation of the above equation, we use the relation between the coupling strength g , the damping rate of the resonator κ , and the detuning Δ at the transition, which is given by Eq. (14). The expansion coefficient a_1 depends on the ratio between coupling and damping rate,

$$\xi = \frac{g^2}{\kappa \Gamma_1}. \quad (22)$$

It grows with increasing g or decreasing κ , which leads to

	Fig. 8 (a) : $\kappa = 5 \times 10^{-4}$	Fig. 8 (b) : $g = 0.003$
curve I: $\xi = 1.125$	$g = 0.003$	$\kappa = 5.0 \times 10^{-4}$
curve II: $\xi = 3.125$	$g = 0.005$	$\kappa = 1.8 \times 10^{-4}$
curve III: $\xi = 8$	$g = 0.008$	$\kappa = 7.2 \times 10^{-5}$
curve IV: $\xi = 18$	$g = 0.012$	$\kappa = 3.1 \times 10^{-5}$

Table I: Parameters in Fig. 8. Here g and κ are in unit of ω_R .

an increased coupling of the amplitude fluctuations and hence increased linewidth.

In the two panels of Fig. 8 we plot the linewidth as a function of the detuning for different g and κ , as obtained in the two approaches. Since the coefficient a_1 depends on the ratio ξ , we choose the parameters such that each curve in Fig. 8 (a) has a corresponding one in Fig. 8 (b) which has the same value for ξ , as shown in Table I. The linewidths represented by curves with the same ratio of coupling to damping rate show similar behavior around the lasing transition. When ξ is small (*e.g.* $\xi = 1.125$), the linewidth grows monotonically with detuning and no peculiar features show up. For larger values of ξ , the linewidth is enhanced around the transition regime, which becomes more pronounced as ξ increases. Moreover, for strong coupling, *e.g.*, for $g/\omega_R = 0.012$, the peak of the linewidth can be even exceed the bare value, $\kappa/2$. In this case, the linewidth at resonance $\kappa_L(\Delta = 0)$ is already comparable to $\kappa/2$.

In the non-lasing regime for strong detuning, the linewidth can be well approximated by [21]

$$\kappa_L = \frac{\kappa}{2} - \frac{g^2 \Gamma_\varphi}{\Gamma_\varphi^2 + \Delta^2} \tau_0 < \frac{\kappa}{2}, \quad (23)$$

approaching the bare linewidth of the resonator, $\kappa/2$, in the infinite detuning limit.

C. Non-exponential decay

Generally, as described in Eq. (17), the emission spectrum $S_e(\omega)$ is the sum of contributions from different eigenvalues. We find that both in the deep lasing and the non-lasing regimes, a single eigenfunction, the one corresponding to the eigenvalue with the smallest real part (denoted as λ_1), is sufficient to describe the spectral properties. In this case, the correlation function of the radiation field decays exponentially in time and the spectrum is a Lorentzian. However, in the transition regime, where the linewidth shows the non-monotonic behavior, more than one eigenfunction contributes to the spectrum.

As a measure of the deviation of the correlation function from the simple exponential form, we define the relative distance between the HWHM linewidth κ_L and the

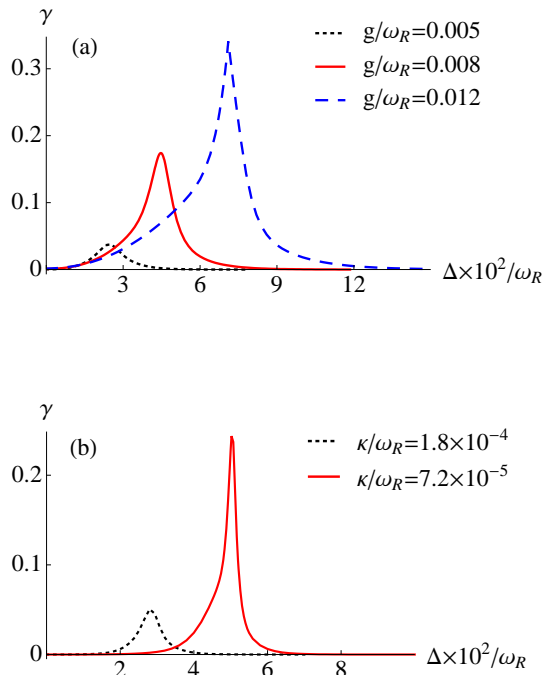


Figure 9: (Color online) Relative distance γ between the HWHM and the real part of the first eigenvalue as a function of the detuning for different values of g with $\kappa/\omega_R = 5 \times 10^{-4}$ (DILE) in panel (a) and for different values of κ with $g/\omega_R = 0.003$ (FPE) in panel (b).

real part of λ_1 ,

$$\gamma = \frac{|\kappa_L - \text{Re}[\lambda_1]|}{\kappa_L}. \quad (24)$$

Fig. 9 shows γ as a function of detuning for different values of g and κ . At resonance (deep lasing regime) and far off-resonance (non-lasing regime) the first eigenvalue is sufficient to describe the linewidth, and the decay of the correlation function is simply exponential. However, when approaching the transition regime where a peak in the linewidth shows up, the weights of further eigenvalues increase, indicating that more eigenvalues must be taken into account. More details are presented in Appendix B.

VI. CONCLUSION

We have studied a single-qubit laser consisting of a qubit coupled strongly to the resonator. The lasing behavior was investigated in a parameter space spanned by the coupling strength g and the detuning Δ . Increasing g or decreasing Δ pushes the system towards the lasing state, characterized by an increase of the average photon number and a decrease of its relative fluctuations.

In single-qubit lasers at low temperature the linewidth of the emission spectrum is dominated by the quantum noise arising from the correlation between the qubit and

the resonator. On resonance, at $\Delta = 0$, the linewidth can be described by the phase diffusion model (PDM) for the phase fluctuations of the laser field. In this case, the emission spectrum is Lorentzian with linewidth simply given by the diffusion coefficient in the Fokker-Planck equation. Away from resonance but still deep in the lasing regime, although the amplitude fluctuations are still weak, their contribution to the linewidth is magnified via the coupling to the phase fluctuations. In this case, the PDM is no longer sufficient.

With increasing coupling strength g or decreasing damping rate of the resonator, the coupling between the phase and amplitude dynamics and, hence, the contribution of amplitude fluctuations to the linewidth becomes stronger. In the transition regime to the lasing state the correlation function of the resonator does not simply decay exponentially in time, and the Fourier transform is no longer Lorentzian. Their behavior is no longer governed by a single eigenvalue λ_1 , distinguished from the other ones by having a much smaller real part. Instead several eigenvalues, with similar real parts, contribute to the spectrum.

In our studies, we employed two complementary approaches in order to cover a wide range of parameters. The DILE method in the Fock state representation is free from approximations on the relative strengths of the coupling, damping rate of the resonator, and that of the qubit. A practical limitation arises from the fact that it can deal only with low photon numbers. In the large-photon number limit, the FPE approach can be employed. The constraint on it is set by the approximation that the coupling strength should be lower than the damping rate of the qubit. In an overlapping parameter regime, where both methods are sufficient, results obtained in the two approaches show good agreement.

Acknowledgements

The authors wish to acknowledge helpful discussions with M. Marthaler and N. Didier. PQJ was supported by the Baden-Württemberg Stiftung via the Kompetenznetz Funktionelle Nanostrukturen. AR acknowledges support by the Humboldt foundation.

Appendix A: FPE in polar coordinates

In polar coordinates, the FPE is given by

$$\begin{aligned} \frac{\partial P(r, \varphi, t)}{\partial t} &= \frac{\kappa}{4r} \frac{\partial}{\partial r} \left\{ [N_{\text{th}} + Q(r) + 2u(r)] r \frac{\partial}{\partial r} \right. \\ &\quad \left. + 4v(r) \frac{\partial}{\partial \varphi} + F(r) \right\} P(r, \varphi, t) \\ &\quad + \kappa \left(D_2(r) \frac{\partial^2}{\partial \varphi^2} + D_1(r) \frac{\partial}{\partial \varphi} \right) P(r, \varphi, t), \end{aligned} \quad (\text{A1})$$

where $u(r)$ and $v(r)$ denote the real and imaginary parts of $e^{-2i\varphi} R$, respectively, and

$$\begin{aligned} F(r) &= r \frac{d}{dr} \left[N_{\text{th}} + Q(r) + 2u(r) \right] \\ &\quad + 2r^2 \left[1 - \frac{C_0}{X(r)} \right] + 4u(r), \\ D_2(r) &= \frac{N_{\text{th}} + Q(r) - 2u(r)}{4r^2}, \\ D_1(r) &= \frac{\Delta C_0}{2\Gamma_\varphi X(r)} + \frac{v(r)}{r^2}, \\ X(r) &= \frac{n_0(\Gamma_\varphi^2 + \Delta^2)}{\Gamma_\varphi^2(n_0 + r^2)}. \end{aligned} \quad (\text{A2})$$

In the steady state we expect the distribution function not to depend on the phase. It can be written in the form of Eq. (11) with

$$\begin{aligned} \Phi(r) &= \ln [N_{\text{th}} + Q(r) + 2u(r)] \\ &\quad + 2 \int dr \frac{r^2 [1 - C_0/X(r)] + 2u(r)}{r [N_{\text{th}} + Q(r) + 2u(r)]}. \end{aligned} \quad (\text{A3})$$

The correlation function of the resonator $\langle a^\dagger(t)a(0) \rangle$ can be obtained by introducing [32],

$$\begin{aligned} W(r, t) &= \int d\varphi d\varphi_0 dr_0 r_0^2 P_s(r_0) \\ &\quad \times e^{i(\varphi_0 - \varphi)} P(r, \varphi, t/r_0, \varphi_0, 0), \end{aligned} \quad (\text{A4})$$

which obeys the differential equation

$$\begin{aligned} \frac{\partial W}{\partial t} &\equiv \hat{L}W \\ &= \frac{\kappa}{4r} \frac{\partial}{\partial r} \left\{ [N_{\text{th}} + Q(r) + 2u(r)] r \frac{\partial}{\partial r} \right. \\ &\quad \left. + 4iv(r) + F(r) \right\} W \\ &\quad + \kappa \left(-D_2(r) + iD_1(r) \right) W. \end{aligned} \quad (\text{A5})$$

We numerically solve this problem by discretizing the amplitude r and diagonalize the \hat{L} matrix on the lattice. We expand $W(r, t)$ in terms of eigenfunctions of

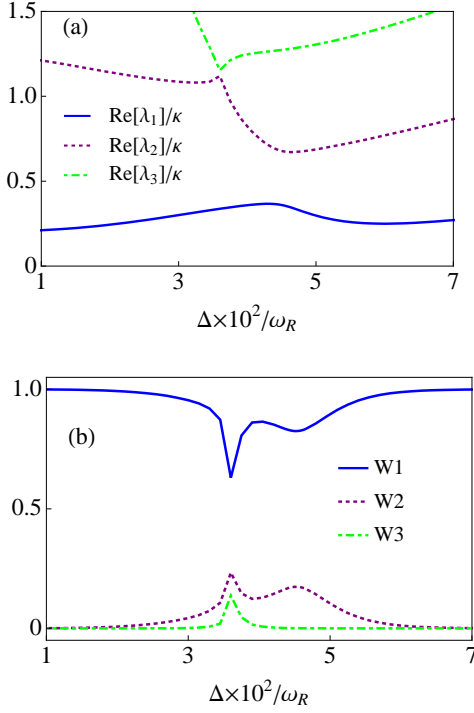


Figure 10: Real parts of the eigenvalues λ_i (panel (a)) and their weights W_i (panel (b)) as function of the detuning. The results are obtained from the DILE method with $\kappa = 5 \times 10^{-4} \omega_R$ and $g = 0.008 \omega_R$.

\hat{L} , namely, $W(r, t) = \sum_n c_n \chi_n(r) e^{\lambda_n t}$ with λ_n being the eigenvalue corresponding to the eigenfunction χ_n . The expansion coefficients are determined by the initial condition $W(r, t = 0) = 2\pi r P_s(r)$.

Appendix B: Eigenvalues contributing to the linewidth

For strong coupling or weak damping of the resonator the linewidth is enhanced around the transition regime. In this case, more than one eigenvalue contribute to the spectrum, and it has no longer a Lorentzian form. Since the eigenvalues with small real parts are of importance for the linewidth, we consider the first three, $\{\lambda_k\}$ (ordered with growing real part). Their weights defined as

$$W_i = \frac{|\alpha_i|^2}{\sum_k |\alpha_k|^2}, \quad (\text{B1})$$

determine how much the corresponding eigenfunctions contribute to the spectrum. As shown in Figs. 10 and 11, when approaching the transition regime, the weight of the first eigenvalue, which dominates in the non-lasing and deep lasing regimes, decreases, while the second or even the third eigenvalues becomes important.

-
- [1] A. Wallraff *et al.*, Nature **431**, 162 (2004).
[2] I. Chiorescu *et al.*, Nature **431**, 159 (2004).
[3] A. Blais *et al.*, Phys. Rev. A, **69** 062320, (2004); R. Schoelkopf and S. Girvin, Nature **451**, 664 (2008).
[4] D. A. Rodrigues, J. Imbers and A. D. Armour, Phys. Rev. Lett. **98**, 067204 (2007).
[5] J. Hauss, A. Fedorov, C. Hutter, A. Shnirman and G. Schön, Phys. Rev. Lett. **100**, 037003 (2008).
[6] M. Marthaler, G. Schön, and A. Shnirman, Phys. Rev. Lett. **101**, 147001 (2008).
[7] O. V. Zhirov and D. L. Shepelyansky, Phys. Rev. Lett. **100**, 014101 (2008).
[8] J. Gambetta *et al.*, Phys. Rev. A **77**, 012112 (2008).
[9] Y. Li *et al.*, Phys. Rev. B, **78** 134301 (2008).
[10] A. Naik *et al.*, Nature **443**, 193 (2006).
[11] J. Johansson *et al.*, Phys. Rev. Lett. **96**, 127006 (2006).
[12] D.I. Schuster *et al.*, Nature **445**, 515 (2007); A. A. Houck *et al.*, Nature **449**, 328 (2007).
[13] M. A. Sillanpää, J. I. Park, and R. W. Simmonds, Nature **449**, 438 (2007); J. Majer *et al.*, Nature **449**, 443 (2007).
[14] O. Astafiev *et al.*, Nature **449**, 588 (2007).
[15] M. Grajcar *et al.*, Nature Physics **4**, 612 (2008).
[16] M. Hofheinz *et al.*, Nature **454**, 310 (2008); J. M. Fink, *et al.*, Nature **454**, 315 (2008).
[17] L.A. Lugiato, Nuovo Cimento **50B**, 89 (1979).
[18] P. D. Drummond and D. F. Walls, Phys. Rev. A **23**, 2563 (1981).
[19] D. Bozyigit *et al.*, arXiv:1002.3738; M. P. da Silva, D. Bozyigit, A. Wallraff, and A. Blais, Phys. Rev. A **82**, 043804 (2010).
[20] S. André, V. Brosco, A. Shnirman, and G. Schön, Phys. Rev. A **79**, 053848 (2009).
[21] S. André, V. Brosco, M. Marthaler, A. Shnirman, and G. Schön, Physica Scripta **T137**, 014016 (2009).
[22] M. O. Scully and M. S. Zubairy, *Quantum Optics*, (Cambridge University Press, Cambridge, UK, 1997).
[23] A. Shnirman, G. Schön, and Z. Hermon, Phys. Rev. Lett. **79**, 2371 (1997).
[24] E. T. Jaynes and F. W. Cummings, Proc. IEEE **51**, 89 (1963).
[25] N. Didier, Ya. M. Blanter, and F. W. J. Hekking, arxiv: 1004.1630 (2010).
[26] U. Fano, Rev. Mod. Phys. **29**, 74 (1957).
[27] C. Cohen-Tannoudji, J. Dupont-Roc, and G. Grynberg, *Atom-Photon Interactions: Basic Processes and Applications* (Wiley, New York, 1992).
[28] C. W. Gardiner and P. Zoller, *Quantum Noise*, (Springer, Berlin, 2004).
[29] C. Ginzel *et al.*, Phys. Rev. A **48**, 732 (1993).
[30] H. J. Carmichael, *Statistical Methods in Quantum Optics 1*, (Springer, Berlin, 2002).
[31] W. H. Louisell, *Quantum Statistical Properties of Radiation*, (John Wiley and Sons, New York, 1990).
[32] R. D. Hempstead and M. Lax, Phys. Rev. **161**, 350 (1967).
[33] H. Haken, *Laser Theory* (Springer-Verlag, Berlin, 1984).

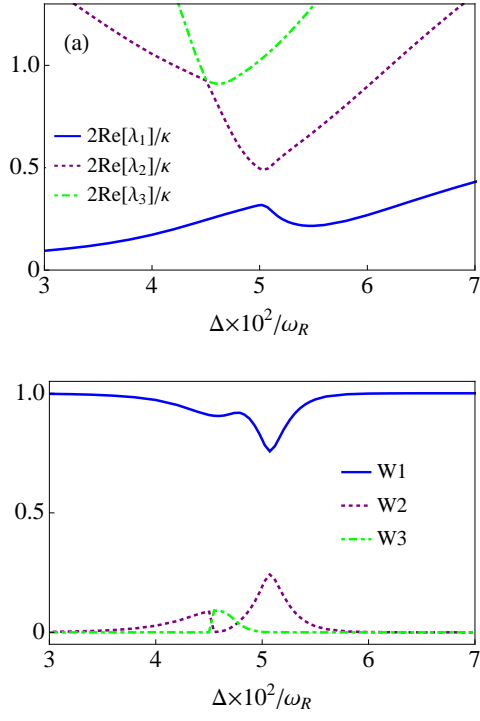


Figure 11: Real parts of the eigenvalues λ_i (panel (a)) and their weights W_i (panel (b)) as function of the detuning. The results are obtained from the FPE method with $\kappa = 7.2 \times 10^{-5} \omega_R$ and $g = 0.003 \omega_R$.